**Steel and Composite Structures**, *Vol. 29, No. 3 (2018) 287-299*
DOI: https://doi.org/10.12989/scs.2018.29.3.287


# Seismic retrofit of a framed structure using damped cable systems

Asad Naeem and Jinkoo Kim *

*Department of Civil Engineering and Architectural Engineering, Sungkyunkwan University, Suwon, Republic of Korea*

(*Received August 20, 2017, Revised August 27, 2018, Accepted September 28, 2018*)

**Abstract.** The purpose of this study is to investigate the effectiveness of damped cable systems (DCS) to mitigate the earthquake-induced responses of a building frame structure. The seismic performance of the DCS is investigated using the fragility analysis and life cycle cost evaluation of an existing building retrofitted with the DCS, and the results are compared with the structure retrofitted with conventional fluid viscous dampers. The comparison of the analysis results reveals that, due to the self-centering capability of the DCS, residual displacement approximately reaches to zero for the structure retrofitted with the DCS. The fragility analysis shows that the structure retrofitted with the DCS has the least probability of reaching the specific limit states compared to the bare structure and the structure with the conventional fluid viscous damper (VD), especially under the severe ground motions. It is also observed that both the initial and the life cycle costs of the DCS seismic retrofitting technique is lesser compare to the structure retrofitted with the VD.

**Keywords:** damped cable system; fragility analysis; life cycle cost; seismic retrofit; self-centering

## 1. Introduction

Self-centering systems have potential for seismic retrofit of structures due to their capability to minimize residual displacement and interstory drift after the structure is shaken by an earthquake. In order to reduce or eliminate residual deformation in structures subjected to seismic loads, many researchers have investigated various self-centering schemes. For example, bracing systems providing stable energy dissipation capacity and a restoring force have been developed (Christopoulos *et al*. 2008, Miller *et al*. 2012, Chou *et al*. 2016). Post-tensioned tendons have been used in prestressed precast shear walls (Bedoya-Ruiz *et al*. 2012), RC moment frames (Rahman and Sritharan 2007, Takeda *et al*. 2013), and steel braced frames (Roke and Jeffers 2012, Dyanati *et al*. 2014, Eatherton *et al*. 2014) to provide both stiffness and restoring force. The superelastic property of the shape memory alloy has been applied to produce damping devices having both energy dissipation and self-centering capacity (Dolce and Cardone 2006, Ingalkar 2014). The hybrid slit damper with shape memory alloy and life cycle cost analysis of the hybrid damper is presented elsewhere (Naeem *et al*. 2017, Nour Eldin *et al*. 2018a).

The seismic performance of combined damping devices has also been investigated as retrofitting techniques for buildings and structures. Tsai *et al*. (1998) combined displacement-dependent and velocity-dependent devices and proposed an economical retrofit solution. The seismic response of steel structures retrofitted with buckling-restrained brace in-series with viscoelastic dampers has been investigated by (Marshall and Charney 2012). Lee and Kim (2015), Lee *et al*. (2017), Kim *et al*. (2017), and Nour Eldin *et al*. (2018b) developed a hybrid damping device by combining steel slit and friction dampers connected in parallel, and showed that the hybrid dampers were especially effective in reducing seismic responses for small to medium earthquakes compared with single dampers with the same yield strength. The mathematical model and seismic control procedure for viscoelastic damper-based retrofit systems are provided in Xu *et al*. (2003, 2004) and Xu *et al*. (2016). Pekcan *et al*. (2000) proposed a supplemental damping device called a damped cable system (DCS) composed of a preloaded viscous damper connected to a prestressed tendon in series. They found that the system is effective under pulse-type ground motions and under service load conditions such as strong wind loads since the system provides high initial stiffness. Sorace and Terenzi (2001, 2012a) further improved the concept by conducting a full-scale dynamic test on a mock building. They developed an analytical model, identified proper structural topologies, and formulated a preliminary sizing criterion of the system. Recently the effectiveness of the damped cable system was evaluated by shaking table tests (Naeen and Kim 2018).

In this study, the seismic performance of the structure retrofitted with the DCS is evaluated and the effectiveness of the DCS is compared to that of the conventional viscous dampers (VD). A parametric study is conducted to show the influence of the damping coefficient of the viscous spring damper, preload, and the size of the cable on the seismic response of the structure. The nonlinear reinforced concrete (RC) framed structure is modeled in the structural analysis software. The analysis results of the model structure after retrofitting with the DCS and the VD are compared. The probabilities of reaching given limit states for the model structures before and after retrofit are compared using

*Corresponding author, Ph.D., Professor,
E-mail: jkim12@skku.edu



ISSN: 1229-9367 (Print), 1598-6233 (Online)

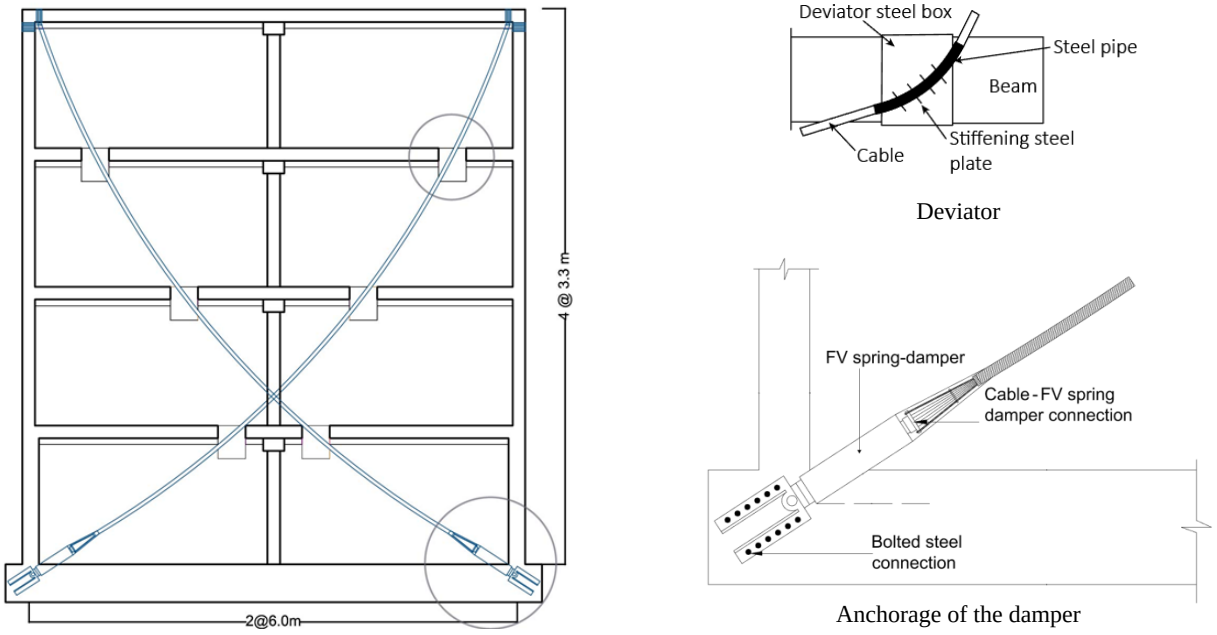


(a) DCS retrofitted structure (b) Components of DCS

Fig. 1 Framed structure installed with DCS

fragility analysis, and the cost-effectiveness of the two retrofitting schemes are investigated by comparing the initial base cost and the life cycle costs analysis.

## 2. Damped cable system

### *2.1 Components*

The geometry layout for a DCS was initially developed by Pekcan *et al*. (2000) for pre-stressed tendon-based fuse-damper (PTFD) system. Sorace and Terenzi (2001, 2012a) provided the preliminary evaluation and further developed the system by using viscous spring dampers instead of fuse steel bars. The DCS includes high-grade steel cables coupled with a viscous damper pressurized with an internal spring, which is fixed to the foundation of the building. The cable is attached to the building using a device called a deviator, which is a steel pipe welded to the steel plate which is bolted or welded the floor of the structure. The cable can slide without friction through the steel pipe. The configuration of a two bay frame installed with the DCS is shown in Fig. 1(a) and the detail drawings of the deviator and the bottom anchorage of the damper to the foundation of the building are presented in Fig. 1(b). The top end of the steel cable is fixed with the steel jaw on one of the upper anchoring floors, while the lower end is tightly connected to the viscous spring damper as shown in Fig. 1(a). The viscous spring damper, which is anchored to the foundation of the building, is preloaded directly at the site during the installation of the DCS. By doing this, the cables are automatically pre-tensioned and the viscous spring dampers are preloaded at their center position. The damper preload activates the damper even when the cable is loosened during earthquakes, and the cable pre-tension provides the self-centering capability of the system. Further details of the DCS structural topologies can be found in Sorace and Terenzi (2012b).

### *2.2 Analytical model of DCS*

The nonlinear behaviour of the DCS is modelled in the structural analysis software SAP2000. Cable is modelled using pre-stressed segments of nonlinear cable element available in the software. The viscous spring damper is modelled according to Kelvin rheological scheme by combining three nonlinear links in parallel as shown in Fig. 2(a). The dashpot link provides the damping while the multi-linear elastic link accounts for the spring's initial and second stiffness. The nonlinear hook link limits the damper device to work in stroke range. The cable is attached in-series with the spring-damper elements as shown in Fig. 2(a). Force-displacement response of a complete assembly is also shown in Fig. 2(b). The forces from cable are transmitted to the floor by the truss action of a 'body constraint' between the centre of curvature and an arbitrary point on the building floor. This configuration can reproduce the behaviour of cable–floor frictionless contact ensuring that the cable moves along the trajectory determined by the deviator (Sorace and Terenzi 2012b).

Sorace and Terenzi (2012b) proposed a criterion for estimating the preliminary size of the DCS including estimation of the cross-sectional area of cable, second stiffness branch of viscous spring damper, and damper and cable preload. Preliminary sizing for retrofit of existing structure begins with estimating the first period of the retrofitted structure. Design of DCS starts by determining the additional lateral stiffness which is necessary to fulfil the requirements of seismic performance in terms of story drifts. Then all design variables of DCS are determined to satisfy the required stiffness. Comprehensive design steps for the DCS are provided in the Sorace and Terenzi (2012b).

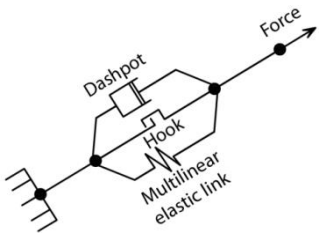


(a) Analysis model

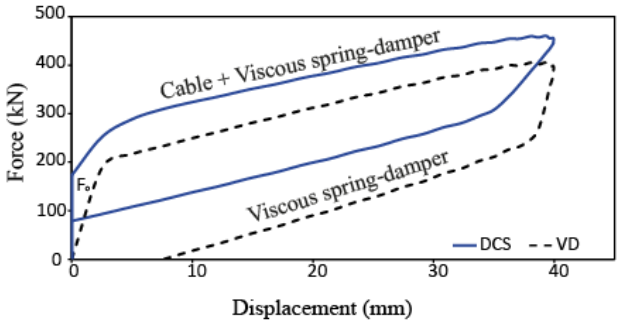


(b) Force-displacement curve

Fig. 2 Analysis model and force-displacement relationship of DCS

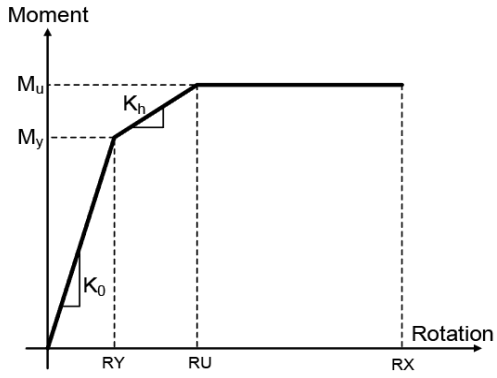


(a) Column

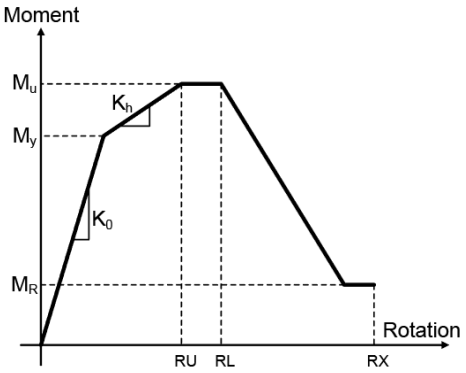


(b) Beam

Fig. 3 Nonlinear moment rotation relationships of structural elements

## 3. Parametric study of DCS

### *3.1 Design of prototype structure*

In this section, the seismic performance of the 2-bay 4-story RC frame shown in Fig. 1(a) is investigated. To verify the effectiveness of the DCS, the analysis results of the bare frame are compared with those of the DCS retrofitted frame. The influence of different parameters of the DCS on the seismic behavior of the structure is also studied in this section. The four-story frame has beam sections of 500 mm × 250 mm and column sections of 400 mm × 450 mm in all stories. The compressive strength of the concrete is taken as 25 MPa, and D-19 reinforcement bars of 280-grade steel are used. The moment frame is designed for gravity loads, resisting the dead load of 7.0 kN/m$^2$ and the live load of 2.0 KN/m$^2$. The sections are assumed to be in cracked conditions and the moment of inertia of the beam and the column sections are reduced to 40% and 70% of those of nominal un-cracked values, respectively. A modal damping of 5% of the critical damping is used in the analyses, and material nonlinearity is accounted for by defining localized plastic hinges at the ends of structural elements. The analysis for beam elements are composed of two end rotation type moment hinges defined based on ASCE/SEI 41-13 (2013). The nonlinear bending moment vs. rotation relationships of beams and columns are represented by tri-linear lines as shown in Figs. 3(a)-(b). The hysteresis loops of the beams and columns used in the dynamic analysis of the model structure are shown in Figs. 4(a) and (b).

### *3.2 Result of dynamic analyses*

The model structure is subjected to three different earthquake records obtained from the PEER NGA database, which are Kern County, Tabas, and Landers earthquakes. The records are scaled to the design spectrum which has the spectral acceleration coefficients of $S_{DS}$ = 0.70 and $S_{D1}$= 0.38 with the site class of 'SD soil' according to the ASCE 7-16 (2016) format. The design spectrum and the response spectra of the three scaled earthquake records are presented in Fig. 5.

The nonlinear time-history analyses (NTHA) of the bare frame and the DCS retrofitted frame are carried out, and the maximum inter-story drift ratio (MIDR) for each ground motion record is plotted in Fig. 6. The analysis results show that the maximum inter-story drift of the bare frame structure for each of the three earthquake records exceeds the limit state of 1.5% of the story height. The DCS based seismic retrofit is carried out so that the maximum lateral drift ratio of the structure becomes less than 1.0 % of the story height. Preliminary design values for the DCS are as follows: cable cross-sectional area Ac is 900 mm$^2$, the preloads for the internal spring and the cables are $F_{0c}$ = $F_{0d}$ =180 kN, and the second stiffness of spring $K_2$ is 6 MN/m. The damping coefficient c is taken as 150 kN (s/m)$^{\alpha}$, where $\alpha$ is taken as 0.2. The analysis results show that the DCS retrofit significantly reduces the inter-story drift below the performance objective of 1% of the story height as shown in Fig. 6. This confirms that the preliminary design values are adequately determined.

The roof displacement time histories of the bare frame and the DCS retrofitted frame subjected to the three ground motions are presented in Fig. 7, which reveals that the

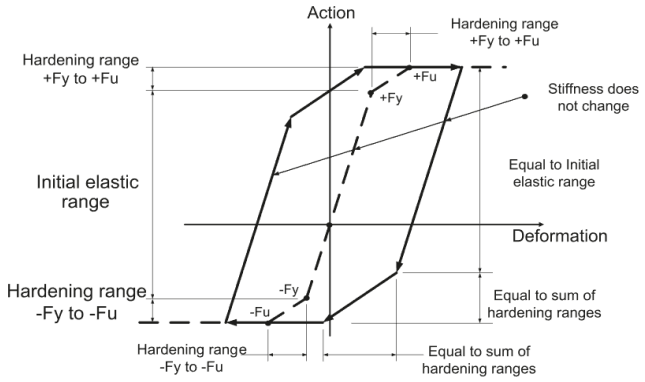


(a) Column

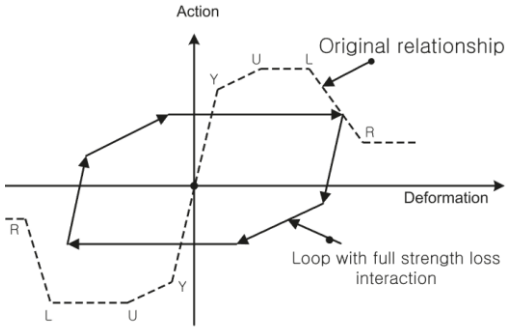


(b) Beam

Fig. 4 Hysteresis loops of RC columns and beams

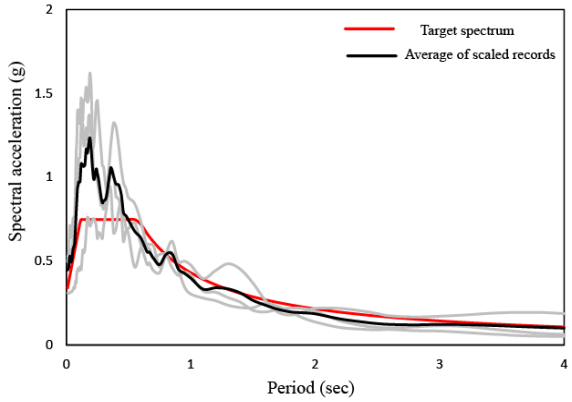


Fig. 5 Response spectra of the ground motions and the target design spectrum

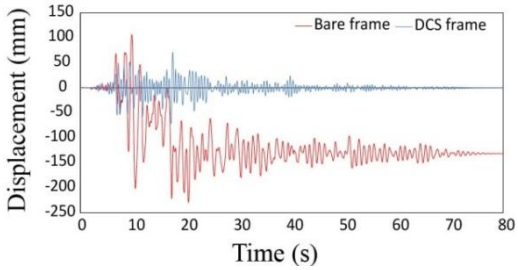


(a)

Fig. 7 Displacement time histories of the model structure subjected to the earthquake records; (a) Kern County (b) Tabas (c) Landers

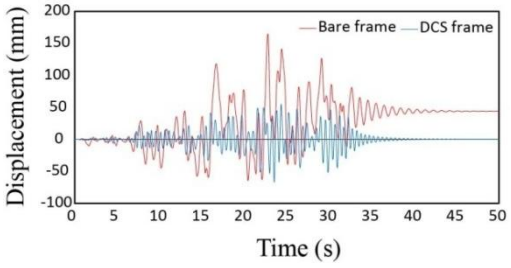


(b)

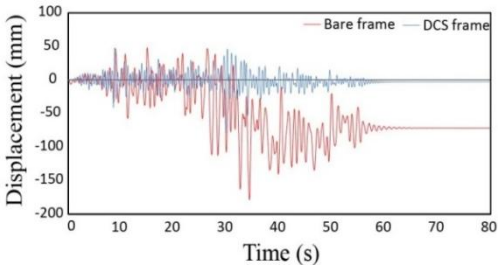


(c)

Fig. 7 Continued

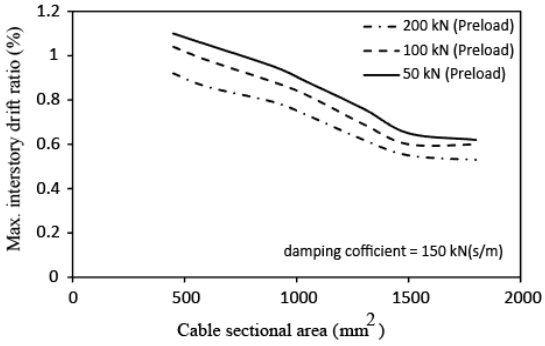


(a) Cable cross-sectional area

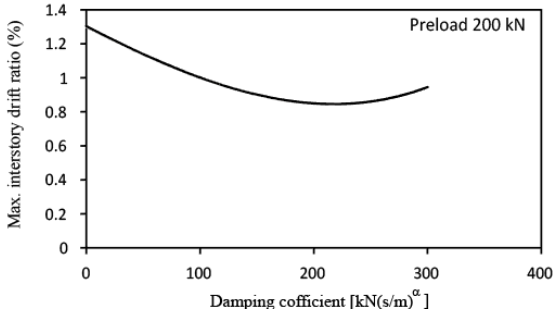


(b) Damping coefficient of the viscous damper

Fig. 8 Variation of the average maximum inter-story drift ratios (MIDR) as a function of design variables

maximum displacements are also reduced more than 50% with the application of the DCS. It can also be observed that the residual displacements of the DCS retrofitted structure almost disappear, mainly due to the self-centering capability of the DCS.

### *3.3 Effect of design variables*

The parametric studies are carried out to observe the

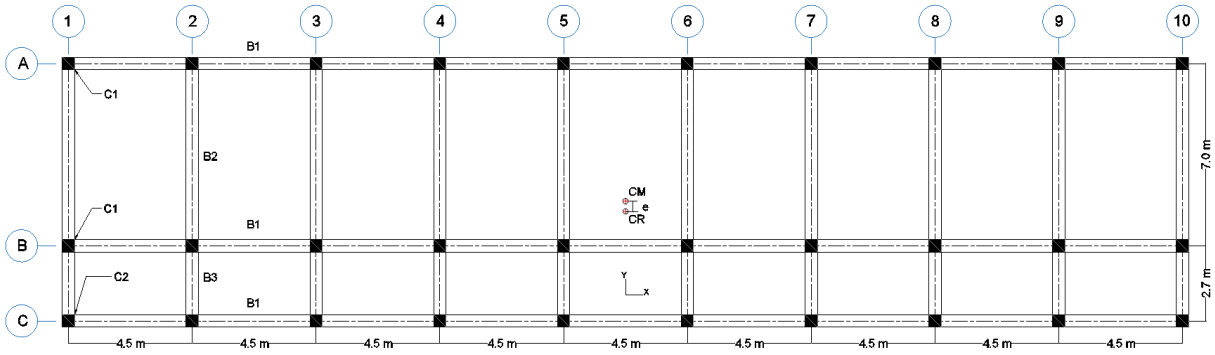


Fig. 9 Typical plan of the analysis model building

influence of the design variables of the DCS, such as the cable cross-sectional area, pre-load, and the damping coefficient of the viscous spring damper. Fig. 8(a) presents the change in the average MIDR of the three ground motions as a function of the cross-sectional area of the cable with three levels of internal spring and cable preloads. The damping coefficient of the viscous spring damper is kept constant of c = 150 kN(s/m)$^{\alpha}$ where $\alpha$ = 0.2. It can be observed that the increment in the cross-sectional area of the cable significantly reduces the MIDR by up to 40%. However as the cable sectional area further increases, the rate of decrease in the response slows down considerably. Fig. 8(b) depicts the variation of the response as a function of the damping coefficient of the viscous spring damper connected to the cable. The preloads of 200 kN are applied to the internal spring and the cable. The curve shows that the MIDR decreases almost linearly until the damping coefficient reaches c = 150 kN (s/m)$^{\alpha}$. It keeps decreasing until it reaches c = 200 kN (s/m)$^{\alpha}$, and then increases slightly after that point. Similar trend is also observed for the maximum roof displacement, which is not shown here for the sake of brevity.

## 4. Seismic retrofit of an existing RC building

### *4.1 Design of the analysis model structure*

The DCS is applied for seismic retrofit of a four-story RC structure designed only for gravity loads based on the assumption that it was built when no seismic design code was applied. Fig. 9 shows the structural plan of the analysis model structure. The dead and live loads of 4.8 kN/m$^2$ and 2.5 kN/m$^2$, respectively, are used in the structural design. The concrete is assumed to have a nominal compressive strength, $f_c$', of 25 MPa with a unit weight of 23.5 kN/m$^3$. The yield stress of reinforcing bars, $f_y$, is 340 MPa. Beam and column reinforcement details are shown in Table 1. The height of each story is 3.3 m, and the sizes of beams and columns are kept constant throughout the height of the structure. The building is assumed to be located on the site class SD soil with the spectral acceleration coefficients of SDS = 0.70 and SD1 = 0.38 according to the ASCE 7-16 (2016) format.

### *4.2 Seismic performance evaluation of the model structure*

The seismic performance assessment of the RC model structure is carried out by nonlinear dynamic time history analysis using the seven earthquake records obtained from the PEER NGA database (2017). Fig. 10 shows the design spectrum and the response spectra of the seven earthquake records scaled to have the same spectral value with the design spectrum at the fundamental period of the structure. Due to the asymmetric plan in the × (long) direction, the centre of mass does not coincide with the centre of stiffness. The analysis results show that the maximum drift ratio between the two corner points is 1.08, which is less than the criterion to be considered as a structure with torsional

Table 1 Reinforcement details of structural elements

| Structural members | | | | |
|---|---|---|---|---|
| | | Longitudinal reinforcement | | |
| Designation | Dimensions(mm) | Top | Bottom | Transverse |
| Beam (B-1) | 550 x 250 | 3 D19 | 3 D19 | D10, 2legs@200mm |
| Beam (B-2) | 500 x 350 | 6 D19 | 6 D19 | D10, 2legs@200mm |
| Beam (B-3) | 500 x 350 | 4 D19 | 4 D19 | D10, 2legs@200mm |

| Designation | Dimensions(mm) | Longitudinal reinforcement | Transverse |
|---|---|---|---|
| Column (C-1) | 450 x 450 | 8 D19 | D10, 2legs@200mm |
| Column (C-2) | 400 x 425 | 8 D19 | D10, 2legs@200mm |

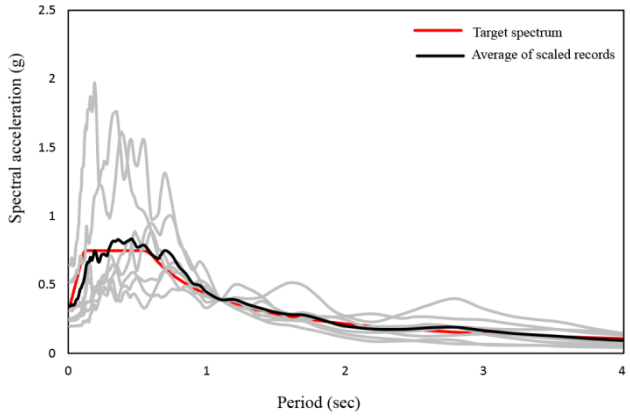


Fig. 10 Response spectra of the seven ground motions and the target design spectrum

irregularity according to ASCE 7-16 (2016).

### *4.3 Seismic retrofit*

Preliminary analysis of the model structure showed that the inter-story drift ratio of the model structure ranged from 1.1% to 1.4% depending on the earthquake used. The DCS-based retrofit design is carried out to limit the MIDR of the model structure within 0.75% of the story height for the given seismic loads. Based on the time history analysis results of the bare frame, the model structure is retrofitted with four pairs of the damped cable system in the longitudinal direction and two pairs of the DCS in the transverse direction using the 'constant horizontal force' layout (Sorace and Terenzi 2012b). The 3-dimensional perspective view of the retrofitted structure is shown in Fig. 11. In the longitudinal direction, the required total cross-sectional area of the cable is determined and is distributed along the stiff and soft side of the structure in such a way that the eccentricity of the retrofitted structure is minimized. The cable cross-sectional area is $A_c$ = 2700 mm$^2$ on the flexible side (side A) and is $A_c$ = 2400 mm$^2$ on the stiff side (side C) shown in Fig. 9. In the transverse direction, cables with a sectional area of 2,100 mm$^2$ are applied on both sides of the building. The preload on the damper and the cable is 300 kN in both directions. The second stiffness branch of $K_2$ = 7 MN/m and damping coefficient c = 200 kN(s/m)$^{\alpha}$ ($\alpha$ = 0.2) are used for the analysis of the retrofitted structure.

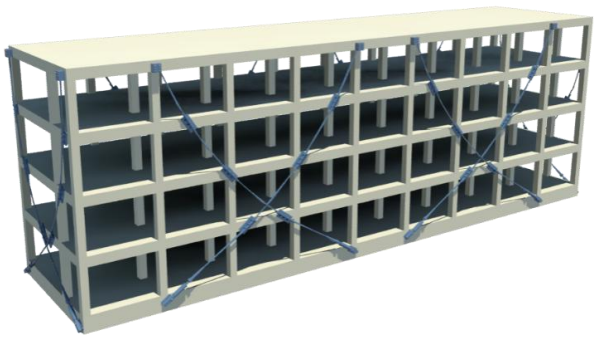

Fig. 11 3-Dimensional perspective view of the model structure retrofitted with DCS

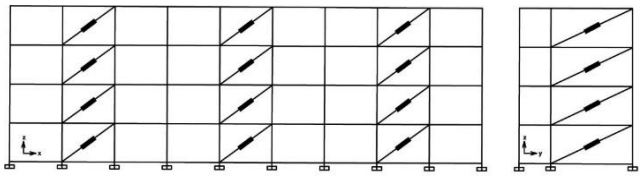

Fig. 12 Locations of the conventional viscous dampers along the longitudinal and transverse directions

For the comparison purpose, the model structure is also retrofitted with conventional fluid viscous dampers (VDs) to satisfy the same target performance. The VDs are distributed on all four sides of the exterior frames of the structure, and the damper locations in both directions are shown in Fig. 12. The required viscous damping needed to retrofit the structure within the target performance point is estimated using the capacity spectrum method (Kim *et al.* 2003). The equivalent viscous damping corresponding to approximately 29% of the critical damping is obtained based on the design procedure. Using the computed equivalent damping, the damping coefficients of the viscous dampers installed in each story are computed from Eq. (1) (ASCE 41-13 2013).

$$\zeta_d = \frac{T\sum_{i=1}^{N} C_i \cos^2\theta_i(\Delta_i - \Delta_{i-1})}{4\pi(\sum_{i=1}^{N} m_i\Delta_i^2)} \quad (1)$$

where $\zeta_d$ is the damping ratio contributed from the viscous dampers, $T$ is the fundamental natural period of the structure, $C_i$ is the damping coefficient of the damper located in the $i^{th}$ story, $\theta$ is the slope of the damper, $m_i$ is the modal mass of the $i^{th}$ story and $\Delta_i$ is the maximum displacement of the $i^{th}$ story. The same damping capacity is located in each story. The damping coefficient $c$ = 290 kN(s/m)$^{\alpha}$ with a velocity exponent of $\alpha$ = 0.2 is computed for the VD to provide the equivalent damping ratio of 29% of critical damping. A total number of 32 viscous dampers are obtained using Eq. (1) to satisfy the target performance objective.

The responses of the structure installed with the DCS and the VD are computed by nonlinear time history analyses using the seven earthquake records, and the results are compared. The roof displacement time histories of the model structure retrofitted with both the DCS and the VD for the seven selected earthquakes are presented in Fig. 13. The analysis results show that the roof displacements of the model structure decrease significantly after retrofitting with either the DCS or the VD. However, comparing the structure retrofitted with the VD, the DCS retrofitted structure experiences notably smaller residual displacements as shown in Fig. 14, which demonstrates the self-centering capability of the damped cable system.

Fig. 15 plots the MIDRs of the model structure before and after retrofit with the DCS and the VD obtained from nonlinear dynamic analyses using the seven earthquake records. It can be noticed that the MIDR of the retrofitted structures is approximately 0.6% in the transverse direction and 0.5% in the longitudinal direction, which are less than

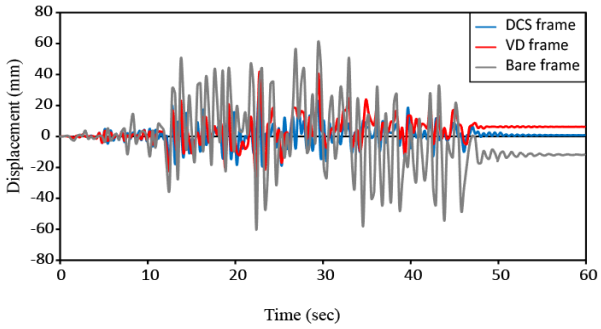


(a) Imperial Valley

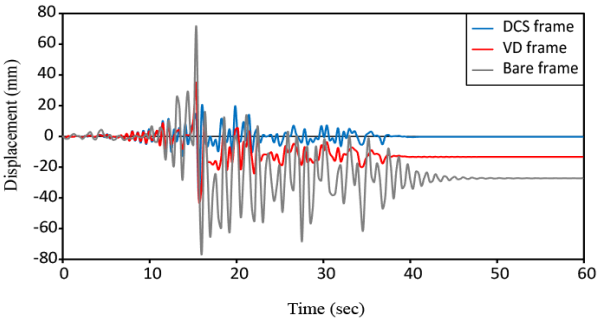


(b) Taiwan

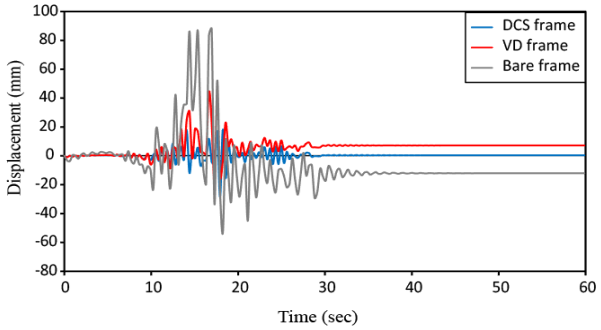


(c) Cape Mendocino

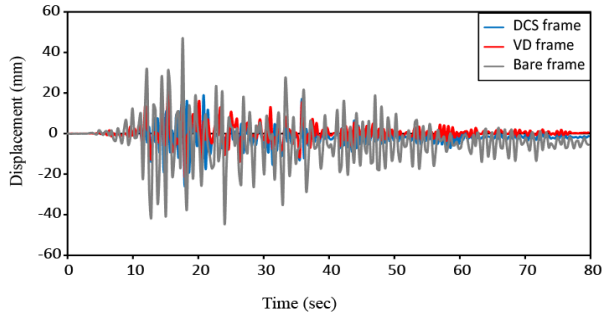


(d) Kern County

Fig. 13 Roof displacement time histories of the model structure before and after retrofit

the target drift ratio of 0.75%. This confirms that the design procedures applied for seismic retrofit produce somewhat conservative results.

Fig. 16 shows the story shear of the model structure before and after the seismic retrofit averaged over the seven earthquake analyses. It can be observed that a significant decrease in story shear is achieved by installing both the damping system.

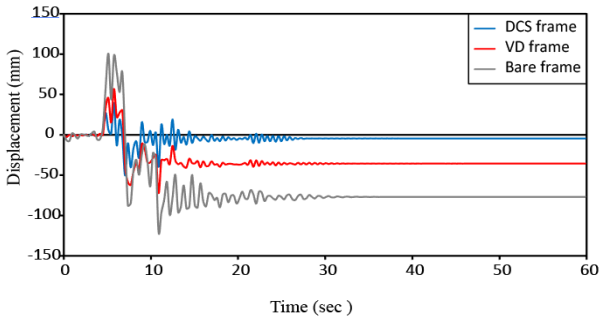


(e) Trinidad

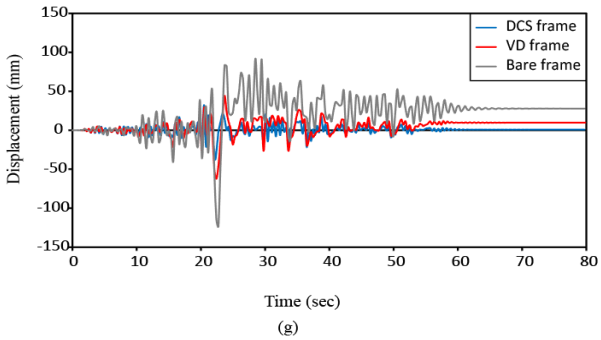


(f) Tabas

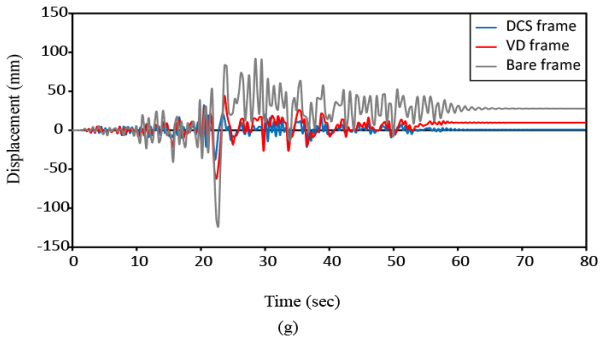


(g) Landers

Fig. 13 Roof displacement time histories of the model structure before and after retrofit

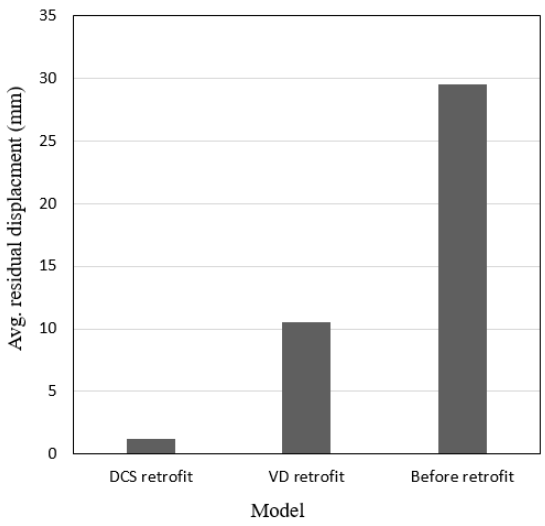


Fig. 14 Mean residual displacement of the model structure before and after retrofit

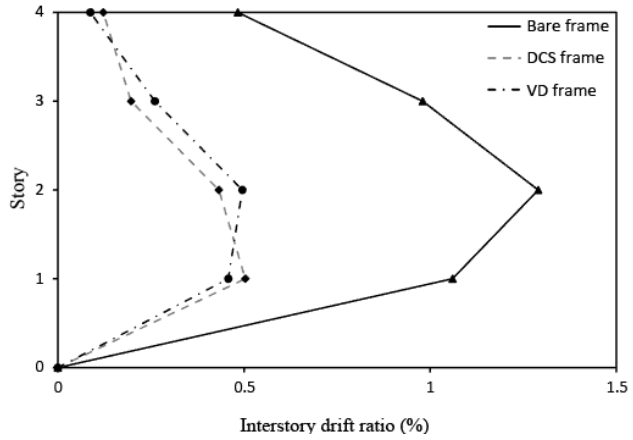


(a) x (long) direction

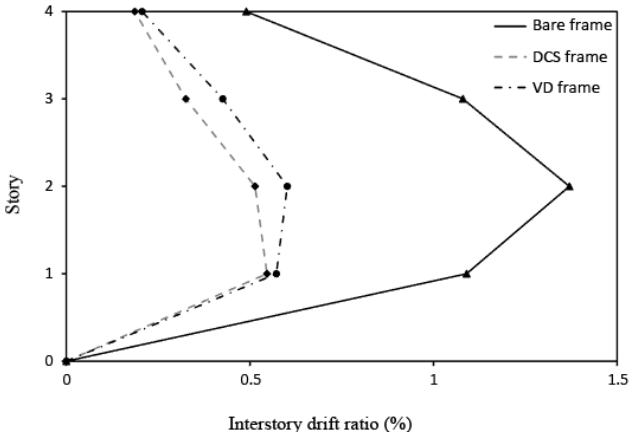


(b) y (short) direction

Fig. 15 Mean inter-story drift ratios of the model structures subjected to the seven earthquake records

The above observation shows that in comparison with the seismic retrofit using VD, in which 32 dampers are used, only 12 viscous spring dampers are applied to produce an equivalent seismic performance. Even though a direct comparison of the retrofit costs of the two different methods

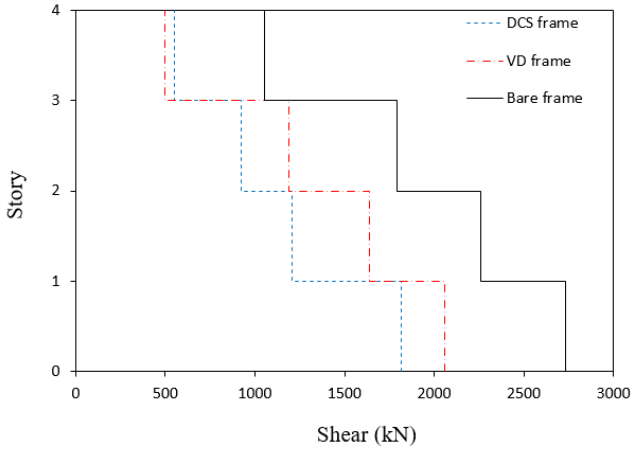


(a) x (long) direction

Fig. 16 Story shear envelopes of the model structures subjected to the seven earthquake records

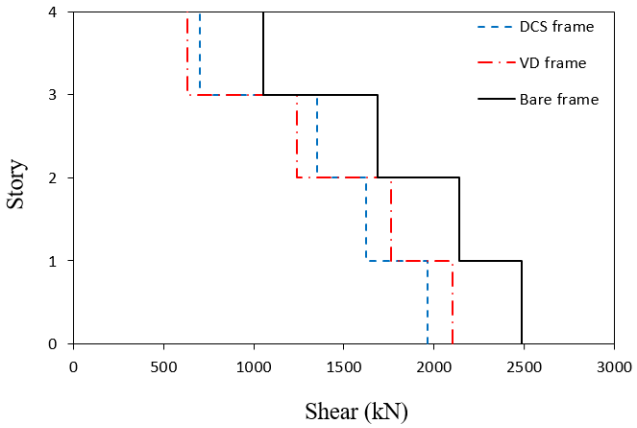


(b) y (short) direction

Fig. 16 Continued

may not be easy, it appears that the DCS method would be more economical than the retrofit method using conventional VD or other types of dampers which need to be stalled in each story.

## 5. Fragility analysis

A seismic fragility curve shows the probability that the response of a structure exceeds a specific limit state when subjected to a ground motion with a specified intensity. In this section, seismic risk assessments of the model structure retrofitted with the DCS and the VD are carried out, and the results are compared with that of the structure before the retrofit. The fragility analysis is carried out using the 22 pairs of far field ground motion records provided in the PEER-NGA database (PEER 2017). For the fragility analysis, the spectral accelerations of the ground motions are scaled in such a way that the spectral accelerations of the ground motions at the fundamental period of the structure are equal to the design spectrum.

The seismic fragility is described by the conditional probability that the structural capacity C fails to resist the structural demand D, given the seismic intensity SI. The fragility curve can be well fitted by a lognormal cumulative distribution function as follows (Celik and Ellingwood 2009)

$$P[C < D \mid SI = x] = 1 - \Phi\left[\frac{\ln\left(\hat{C}/\hat{D}\right)}{\sqrt{\beta_{D/SI}^2 + \beta_C^2 + \beta_M^2}}\right] = 1 - \Phi\left[\frac{\ln\left(\hat{C}/\hat{D}\right)}{\beta_{TOT}}\right] \quad (2)$$

where $\Phi[\cdot]$ is the standard normal cumulative distribution function, $\hat{C}$ is the median structural capacity associated with the limit state, $\hat{D}$ is the median structural demand . The uncertainties in seismic risk assessment are considered in $\beta_{TOT}$ which consists of the uncertainty in the capacity $\beta_C$, uncertainty in the structural demand $\beta_{D/SI}$, and modeling uncertainties $\beta_M$. In this study the total system collapse uncertainty $\beta_{TOT}$ is assumed to be 0.6 according to FEMA P695 (2009).

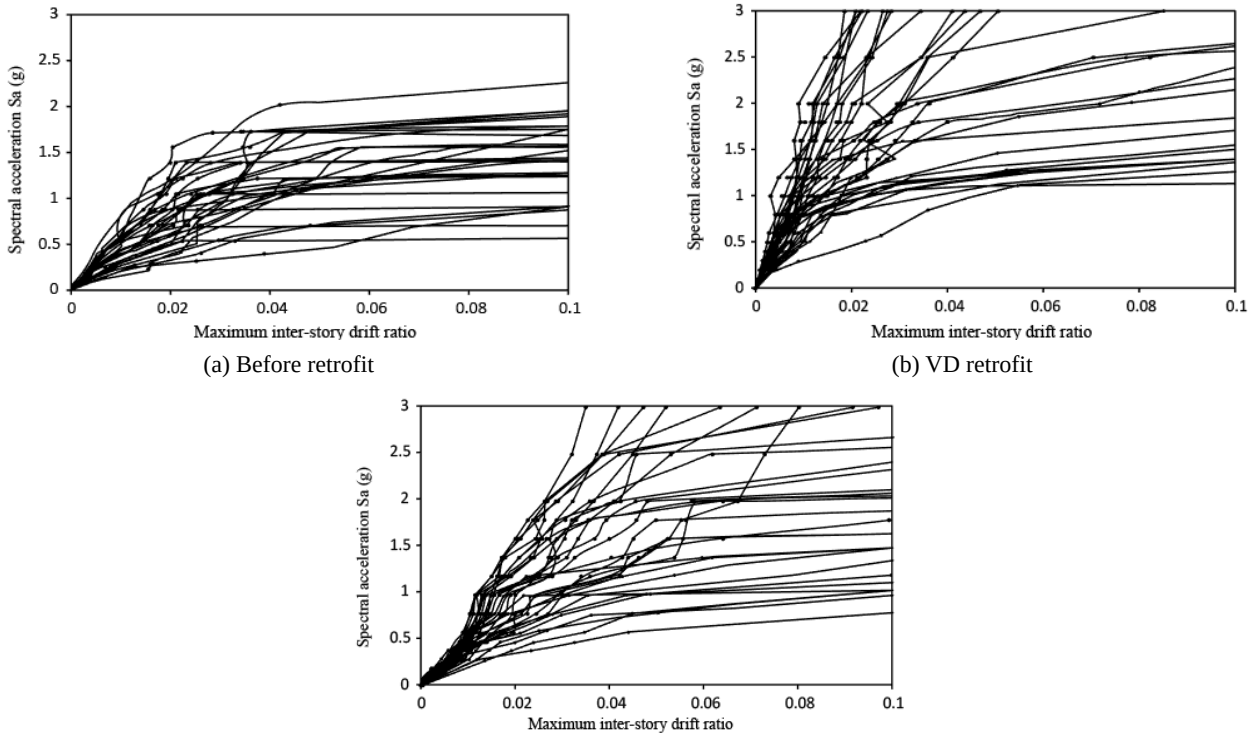


(a) Before retrofit

(b) VD retrofit

(c) DCS retrofit

Fig. 17 Incremental dynamic analysis results of the model structures

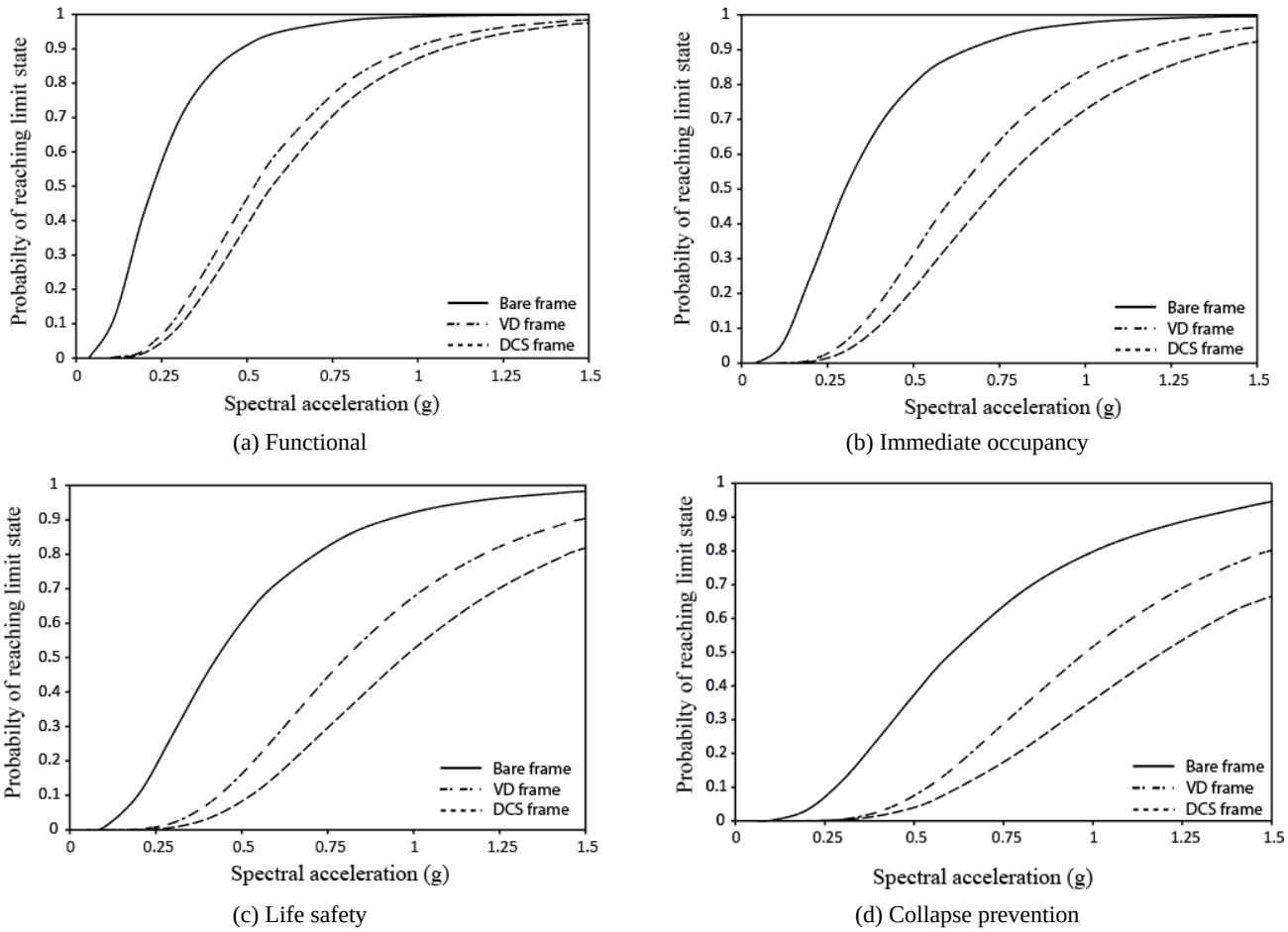


(a) Functional

(b) Immediate occupancy

(c) Life safety

(d) Collapse prevention

Fig. 18 Fragility curves of the model structures corresponding to the limit states

Incremental dynamic analyses (IDA) of the structure before and after the seismic retrofit subjected to the 22 pairs of earthquake records are conducted first to obtain the statistical distribution of the dynamic response. Fig. 17 shows the spectral acceleration *vs*. mean interstory drift ratios obtained from IDA of the model structures. It can be observed that, for a given spectral acceleration, the inter-story drift of the structure decreases after retrofit with the DCS and VD. Based on the IDA results, the probability of reaching the limit states which are functional, immediate occupancy (IO), life safety (LS), and collapse prevention (CP) are obtained for the analysis model. In this study, the limit states for the Functional, IO, LS, and CP are defined as the maximum inter-story drift ratio corresponding to 0.75%, 1.0%, 1.5%, and 2.5% of the story height, respectively. The fragility curves for the model structure before and after the seismic retrofit corresponding to the limit states are presented in Fig. 18.

The fragility curves demonstrate that the bare frame has the highest probability of reaching all the limit states. However, the difference in the failure probability becomes smaller as limit states change from Functional to CP. It can be noted that the DCS frame exhibits the lowest failure probabilities compared to the bare frame and the VD frame. In the case of the Functional limit state, the failure probability for the DCS frame and the VD frame are almost similar for low intensities, but the difference increases with an increase in the seismic intensity. It is interesting to note that the difference of failure probabilities between the DCS retrofitted frame and the VD retrofitted frame, increases from the IO to CP limit state. It can be inferred that the DCS-based retrofit can be more effective in enhancing the seismic safety under medium and severe ground motion levels.

The median failure intensity (i.e., the seismic intensity corresponding to 50% probability of failure) of the structure before retrofit is 0.23 g for Functional, 0.30 g for IO, 0.44 g for LS, and 0.57 g for CP limit states. The significant improvement in the seismic performance can be observed after the retrofit with the DCS, the median failure intensity of the DCS frame increases to 0.58 g, 0.74 g, 0.97 g and 1.24 g for the Functional, IO, LS and CP limit states respectively. Comparing the fragility curves of the bare structure and the DCS retrofitted structure shows that the probability of reaching each limit state at the design level spectral acceleration decreases from 86% to 41% for Functional, 73% to 26% for IO limit state. Similarly, the reduction in the probability of reaching LS and CP limit states is from 52% to 12% and from 32% to 7.0%, respectively. The fragility curves also show that the difference between the median failure intensities of the structure retrofitted with the DCS and VD increases as the limit states changes from IO to CP. The difference of the median failure intensity for the DCS and VD retrofitted structure is 6.5% for Functional and 13.5 % for IO limit state. The difference increases significantly to 19% for the LS and 22% for CP limit state. The observations from the fragility analysis indicate that the installation of the damped cable system is more efficient retrofit solution for severe and medium earthquakes compared to the retrofit with conventional viscous dampers.

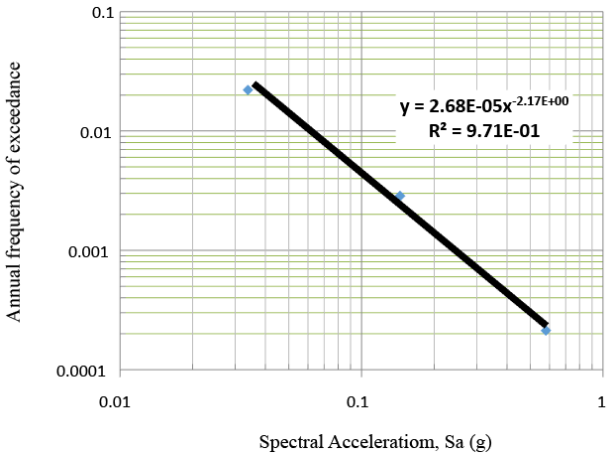


Fig. 19 Seismic hazard curve used in LCC evaluation

## 6. Expected life cycle cost of the retrofitted structures

The estimation of the lifetime cost in earthquake engineering is used to quantify the economic losses in relation to the structural response. To compute the damage cost of a structure subjected to a seismic load, the damage state probability and the annual probability of exceeding a selected limit state need to be obtained. Cornell *et al*. (2002) provides the following equation for computing the damage state probability $P_{LS}$

$$P_{LS} = H\left(S_a^{\hat{C}}\right) exp\left[\frac{1}{2}\frac{k^2}{b^2}\left(\beta_{D|S_a}^2 + \beta_C^2\right)\right] \tag{3}$$

where $S_a^{\hat{C}}$ is the spectral acceleration corresponding to the median drift capacity obtained from the fragility curve; $H(S_a^{\hat{C}})$ is the annual probability of exceedance at intensity $S_a$ for a given site, shown in Fig. 19; $k$ and $b$ are the linear regression coefficients of the hazard and the drift demand on intensity $S_a$ in logarithmic space; $\beta_{D|S_a}$ is the dispersion measure for the drift demand $D$ at given $S_a$; and $\beta_c$ is the dispersion measure for drift capacity $C$ (standard deviation of natural logarithm) assumed to be 0.3 based on previous studies (Cornell *et al*. 2002). Corresponding to the damage state probabilities computed, the expected life cycle cost (LCC) of a structure can be calculated as follows (Wen and Kang 2001)

$$E[C_{LC}] = C_o + \int_0^L E[C_{SD}]\left(\frac{1}{1+\lambda}\right)^t dt = C_o + \alpha L E[C_{SD}] \tag{4}$$

where $C_o$ is the initial construction cost, $L$ is the service life of the structure, $\lambda$ is the annual discount rate, and $E[C_{SD}]$ is the annual expected seismic damage cost which is governed by a Poisson process and does not depend on time. It is assumed that structural capacity does not degrade over time and the structure is restored to its original condition after each hazard. The parameters $\alpha$, $q$ and $E[C_{SD}]$ can be formulated as

$$\alpha = [1 - \exp(-ql)/ql] \tag{5}$$

$$q = ln\ (1+ \lambda) \tag{6}$$

$$E[C_S D] = \Sigma_{(i=1)}^{N} C_i P_i \tag{7}$$

where $N$ is the total number of limit-states considered, $P_i$ is the total probability that the structure is in the $i^{th}$ damage state throughout its lifetime, and $C_i$ is the corresponding cost. In accordance with the definition of seismic hazard, three structural damage states are used (i.e. $N$ is equal to three) such as IO, LS, and CP. $C_i$ is assumed to be 30, 70 and 100% of the initial cost of the structure, respectively, for the three limit states considered. $P_i$ is given by

$$P_i = P\left(\Delta_D > \Delta_{C,i}\right) - P(\Delta_D > \Delta_{C,i+1}) \tag{8}$$

where $\Delta_D$ is the earthquake demand and $\Delta_{C,i}$ is the structural capacity, usually represented in terms of drift ratio, defining the $i^{th}$ damage state. The probability of demand being greater than capacity, $\delta_D > \delta_{C,i}$, is evaluated as discussed in the previous step.

The cost of the structure is assumed to be 1,030 \$/m$^2$ according to Turner and Townsend (2016). This leads to the initial building cost of \$ 1,612,427 before seismic retrofit. A single unit of preloaded viscous spring damper used in the DCS is assumed to be \$ 14,200 including the costs for removing existing non-structural elements and installation of the device. The cost of a single unit of the viscous damper is assumed to be \$ 11,000 including removing and installation cost.

This leads to the total retrofit costs of \$ 352,000 (32 units) and \$ 222,600 (12 units) for the VD and DCS retrofit, respectively. This leads to the total initial costs (building cost + retrofit cost) of \$1,964,427 and \$ 1,828,427 for the structure retrofitted with VD and DCS, respectively, as depicted in Fig. 20. This shows that the initial base cost of the structure retrofitted with DCS is slightly smaller than that of the model structure retrofitted with the VD.

The expected repair costs of the model structure before and after the seismic retrofit are presented in Figs. 21(a) and (b), respectively, for the three limit states. It can be observed that the damage costs reduce significantly in the structure with the seismic retrofit. Comparing the two

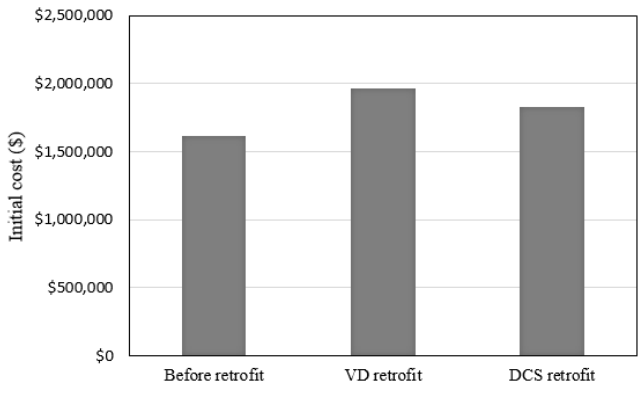


Fig. 20 Initial cost of the model structure before and after seismic retrofit

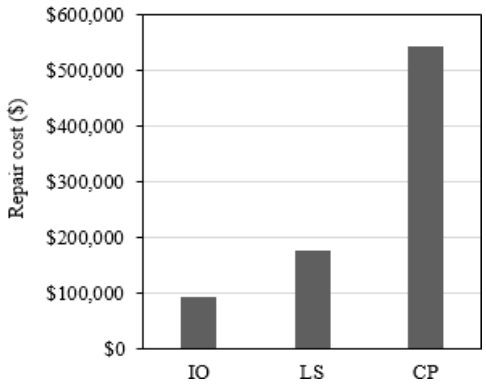


(a) Before retrofit

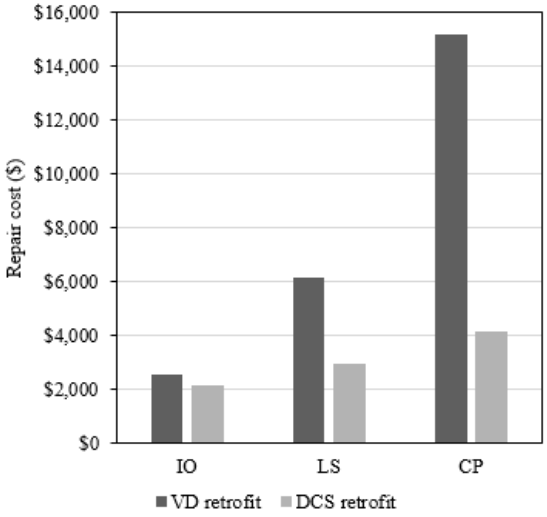


(b) After retrofit

Fig. 21 Repair costs of the model structure before and after the seismic retrofit at the three limit states

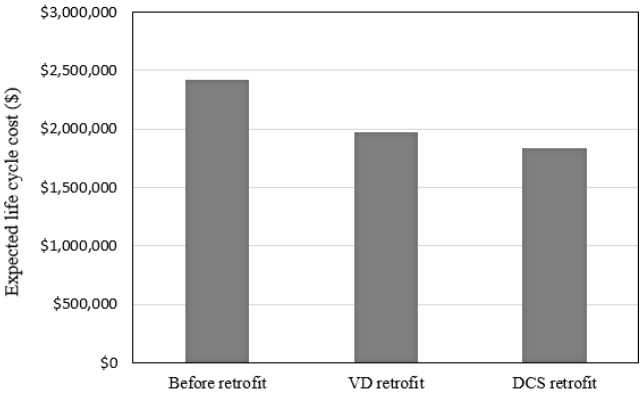


Fig. 22 Expected life cycle cost of the model structures for the building life span of 60 years

retrofitting schemes, smaller damage costs are estimated in the structure retrofitted with the DCS. The difference in repair cost is most significant in the CP limit state. The expected life cycle costs (initial cost + repair cost) of the model structure for the 60 year building life span are depicted in Fig. 22. Table 2 shows the parameters used in the LCC evaluation of the model structures. The

Table 2 Parameters used for life cycle cost evaluation

| Structure | Bare frame | | | VD frame | | | DCS frame | | |
|---|---|---|---|---|---|---|---|---|---|
| Limit state | IO | LS | CP | IO | LS | CP | IO | LS | CP |
| $S_A^{\hat{C}}$ (g) | 0.30 | 0.44 | 0.57 | 0.63 | 0.80 | 0.97 | 0.74 | 0.97 | 1.19 |
| $\beta_{D\|Sa}$ | 0.29 | 0.40 | 0.82 | 0.26 | 0.31 | 0.45 | 0.18 | 0.29 | 0.34 |
| H ($S_a$) | 0.0004 | 0.0002 | 0.00019 | 0.000052 | 0.000052 | 0.000023 | 0.000011 | 0.000011 | 0.00001 |
| $k_o$ | | 0.0000268 | | | 0.0000268 | | | 0.0000268 | |
| t (years) | | 60 | | | 60 | | | 60 | |
| k | | 2.20 | | | 2.20 | | | 2.20 | |
| b | | 2.20 | | | 2.20 | | | 2.20 | |
| $\beta_c$ | | 0.3 | | | 0.3 | | | 0.3 | |
| $P(L_S \|_{Sa})$ | 0.68 | 0.51 | 0.12 | 0.080 | 0.082 | 0.051 | 0.015 | 0.012 | 0.012 |
| LCC ($) | | 2,426,397 | | | 1,973,752 | | | 1,830,613 | |
| Difference w.r.t the bare frame | | - | | | 18.6% | | | 25.5% | |

expected repair cost of the structure without retrofit is estimated to be $ 813,970 for the given building life span, and those of the structure retrofitted with VD and DCS are significantly reduced to $ 19,920 and $ 9,240, respectively. It can be observed that the structure without seismic retrofit has the highest lifetime cost, whereas the DCS retrofitted structure exhibits the smallest expected LCC followed by the structure retrofitted with the VD. More precisely, the life cycle costs of the model structure retrofitted with the viscous dampers and DCS are 18.7% and 25.5% smaller than that of the structure without retrofit, respectively. In comparison with the initial costs, in which the DCS retrofitted structure is 6.9% cheaper than that of the structure retrofitted with VD, the LCC of the DCS retrofitted structure turns out to be 7.3% smaller than that of the structure retrofitted with VD. This implies that the DCS with added stiffness and self-centering capability will be more effective in terms of the life cycle cost.

## 7. Conclusions

The present study investigated the seismic performance of the damped cable system which utilizes added stiffness and damping combined with the self-centering capability to reduce the response of structures when subjected to earthquake ground motion. A parametric study was carried out on the RC plane frame to examine the effects of the mechanical and geometrical properties of the DCS. A RC framed structure was analyzed as a case study before and after the seismic retrofit, and the results were compared with those of the structure retrofitted with conventional viscous dampers.

The parametric study showed that the cross-sectional area of the cables affected the seismic performance of the DCS significantly, and the seismic response generally decreased as the cable cross-sectional area increased. The damping coefficient of the viscous spring damper connected to the cable turned out to have an optimal range for reducing the seismic responses. The increase in the pretension of a cable also assisted in reducing the response.

The nonlinear dynamic analysis results of the model structure showed that the DCS retrofit resulted in relatively small residual displacement, due to self-centering capability. The results also showed that the target performance could be achieved with the DCS retrofit using a fewer number of damper units compared to the conventional VD retrofit. The fragility curves showed that the DCS retrofit resulted in the least probability of failure for all limit states considered compared to the VD retrofitted structure and bare frame. The relative effectiveness of the DCS was more significant under severe earthquakes than under the small or moderate earthquakes. The life cycle cost evaluation showed that the DCS with self-centering capability would be more cost effective for seismic retrofit of building structures.

## Acknowledgments

This research was supported by a grant (code 17CTAP-C132889-01) from Technology Advancement Research Program (TARP) funded by Ministry of Land, Infrastructure and Transport of Korean government.

## References

ASCE/SEI 7-16 (2016), American Society of Civil Engineers; Minimum Design Loads for Buildings and Other Structures, Reston, FL, USA.

ASCE/SEI 41-13 (2013), American Society of Civil Engineers; Seismic Evaluation and Retrofit of Existing Buildings, Reston, FL, USA.

Bedoya-Ruiz, D.A., Bermúdez, C.A., Á lvarez, D.A., Ortiz, G.A. and Escobar, J.V. (2012), "Cyclic behavior of prestressed precast concrete walls", *Proceedings of 15th WCEE*, Lisbon, Portugal.

Celik, O.C. and Ellingwood, B.R. (2009), "Seismic risk assessment of gravity load designed reinforced concrete frames subjected to Mid-America ground motions", *J. Struct. Eng.*,

**135**(4), 414-424.
Chou, C.C., Tsai, W.J. and Chung, P.T. (2016), "Development and validation tests of a dual-core self-centering sandwiched buckling-restrained brace (SC-SBRB) for seismic resistance", *J. Struct. Eng.*, **121**, 30-41.
Christopoulos, C., Tremblay, R., Kim, H.J. and Lacerte, M. (2008), "Self-centering energy dissipative bracing system for the seismic resistance of structures development and validation", *J. Struct. Eng.*, **134**(1), 96-107.
Cornell, C.A., Jalayer, F., Hamburger, R.O. and Foutch, D.A. (2002), "Probabilistic basis for the 2000 SAC Federal Emergency Management Agency steel moment frame guidelines", *J. Struct. Eng.*, **128**(4), 526-533.
Dolce, M. and Cardone, D. (2006), "Theoretical and experimental studies for the application of shape memory alloys in civil engineering", *J. Eng. Mater. Technol.*, **128**(3), 302-311.
Dyanati, M., Huang, Q. and Roke, D.A. (2014), "Structural and nonstructural performance evaluation of self-centering, concentrically braced frames under seismic loading", In: *Structures Congress 2014*, pp. 2393-2404.
Eatherton, M.R., Ma, X., Krawinkler, H., Mar, D., Billington, S., Hajjar, J.F. and Deierlein, G.G. (2014), "Design concepts for controlled rocking of self-centering steel-braced frames", *J. Struct. Eng.*, **140**(11), 04014082.
FEMA P695 (2009), Quantification of Building Seismic Performance Factors; Federal Emergency Management Agency (FEMA), FEMA, USA.
Ingalkar, R.S. (2014), "Rehabilitation of Buildings and Bridges by Using Shape Memory Alloys (SMA)", *Int. J. Civil Eng. Res.*, **5**(2), 163-168.
Kim, J., Choi, H. and Min, K.W. (2003), "Performance-based design of added viscous dampers using capacity spectrum method", *J. Earthq. Eng.*, **7**(1), 1-24.
Kim, J., Kim, M. and Nour Eldin, M. (2017), "Optimal distribution of steel plate slit dampers for seismic retrofit of structures", *Steel Compos. Struct., Int. J.*, **25**(4), 473-484
Lee, J. and Kim, J. (2015), "Seismic performance evaluation of moment frames with slit-friction hybrid dampers", *Earthq. Struct., Int. J.*, **9**(6), 1291-1311.
Lee, J., Kang, H. and Kim, J. (2017), "Seismic performance of steel plate slit-friction hybrid dampers", *J. Constr. Steel Res.*, **136**, 128-139.
Marshall, J.D. and Charney, F.A. (2012), "Seismic response of steel frame structures with hybrid passive control systems", *Earthq. Eng. Struct. Dyn.*, **41**(4), 715-733.
Miller, D.J., Fahnestock, L.A. and Eatherton, M.R. (2012), "Development and experimental validation of a nickel–titanium shape memory alloy self-centering buckling-restrained brace", *Eng. Struct.*, **40**, 288-298.
Naeem, A. and Kim, J. (2018), "Seismic performance evaluation of a spring viscous damper cable system', *Eng. Struct.*, **176**, 455-467.
Naeem, A., Nour Eldin, M., Kim, J. and Kim, J. (2017), "Seismic performance evaluation of a structure retrofitted using steel slit dampers with shape memory alloy bars", *Int. J. Steel Struct.*, **17**(4), 1627-1638.
Nour Eldin, M., Naeem, A. and Kim, J. (2018a), "Life-cycle cost evaluation of steel structures retrofitted with steel slit damper and shape memory alloy–based hybrid damper", *Adv. Struct. Eng.*, 1369433218773487.
Nour Eldin, M., Kim, J.G. and Kim, J. (2018b), "Optimum distribution of steel slit-friction hybrid dampers based on life cycle cost", *Steel Compos. Struct., Int. J.*, **27**(5), 633-646.
PEER (2017), PEER NGA Database, Pacific Earthquake Engineering Research Center, University of California, Berkeley, CA, USA. http://peer.berkeley.edu/nga
Pekcan, G., Mander, J.B. and Chen, S.S. (2000), "Balancing lateral loads using tendon-based supplemental damping system", *J. Struct. Eng.*, **126**(8), 896-905.
Rahman, M.A. and Sritharan, S. (2007), "Performance-based seismic evaluation of two five-story precast concrete hybrid frame buildings", *J. Struct. Eng.*, **133**(11), 1489-1500.
Roke, D. and Jeffers, B. (2012), "Parametric study of self-centering concentrically-braced frame systems with friction-based energy dissipation", *Proceeding of Behaviour of Steel Structures in Seismic Areas* (*STESSA*), pp. 691-696.
Sorace, S. and Terenzi, G. (2001), "Non-linear dynamic modelling and design procedure of FV spring-dampers for base isolation", *Eng. Struct.*, **23**(12), 1556-1567.
Sorace, S. and Terenzi, G. (2012a), "The damped cable system for seismic protection of frame structures. Part I: General concepts, testing, and modeling", *Earthq. Eng. Struct. Dyn.*, **41**(5), 915-928.
Sorace, S. and Terenzi, G. (2012b), "The damped cable system for seismic protection of frame structures. Part II: Design and application", *Earthq. Eng. Struct. Dyn.*, **41**(5), 929-947.
Tsai, C., Chen, K. and Chen, C. (1998), "Seismic resistibility of high-rise buildings with combined velocity-dependent and velocity-independent devices", *ASME-PUBLICATIONS-PVP* **366**, 103-110.
Turner & Townsend (2016), International Construction Cost Survey 2016-2017.
Wen, Y.K. and Kang, Y.J. (2001), "Minimum building life-cycle cost design criteria I: Methodology", *J. Struct. Eng.* (*ASCE*), **127**(3), 330-337.
Xu, Z.D., Shen, Y.P. and Zhao, H.T. (2003), "A synthetic optimization analysis method on structures with viscoelastic dampers", *Soil Dyn. Earthq. Eng.*, **23**(8), 683-689.
Xu, Z.D., Zhao, H.T. and Li, A.Q. (2004), "Optimal analysis and experimental study on structures with viscoelastic dampers. Journal of Sound and Vibration", **273**(3), 607-618.
Xu, Z.D., Liao, Y.X., Ge, T. and Xu, C. (2016), "Experimental and theoretical study of viscoelastic dampers with different matrix rubbers", *J. Eng. Mech.*, **142**(8), 04016051.

*CC*